Oxyhalogen−Sulfur Chemistry: Kinetics and Mechanism of Oxidation of *N*-Acetylthiourea by Chlorite and Chlorine Dioxide[1]

Olufunke Olagunju,[†,‡] Paul D. Siegel,[‡] Rotimi Olojo,[†] and Reuben H. Simoyi*[,†]

Department of Chemistry, Portland State University, Portland, Oregon 97207-0751, and National Institute for Occupational Safety and Health, Health Effects Laboratory Division, 1095 Willowdale Road, Morgantown, West Virginia 26506

Received: October 11, 2005; In Final Form: November 30, 2005

The oxidation reactions of *N*-acetylthiourea (ACTU) by chlorite and chlorine dioxide were studied in slightly acidic media. The ACTU−ClO_2^- reaction has a complex dependence on acid with acid catalysis in pH > 2 followed by acid retardation in higher acid conditions. In excess chlorite conditions the reaction is characterized by a very short induction period followed by a sudden and rapid formation of chlorine dioxide and sulfate. In some ratios of oxidant to reductant mixtures, oligo-oscillatory formation of chlorine dioxide is observed. The stoichiometry of the reaction is 2:1, with a complete desulfurization of the ACTU thiocarbamide to produce the corresponding urea product: $2ClO_2^- + CH_3CONH(NH_2)C{=}S + H_2O \rightarrow CH_3CONH(NH_2)C{=}O + SO_4^{2-} + 2Cl^- + 2H^+$ (A). The reaction of chlorine dioxide and ACTU is extremely rapid and autocatalytic. The stoichiometry of this reaction is $8ClO_2(aq) + 5CH_3CONH(NH_2)C{=}S + 9H_2O \rightarrow 5CH_3CONH(NH_2)C{=}O + 5SO_4^{2-} + 8Cl^- + 18H^+$ (B). The ACTU−ClO_2^- reaction shows a much stronger HOCl autocatalysis than that which has been observed with other oxychlorine−thiocarbamide reactions. The reaction of chlorine dioxide with ACTU involves the initial formation of an adduct which hydrolyses to eliminate an unstable oxychlorine intermediate $HClO_2^-$ which then combines with another ClO_2 molecule to produce and accumulate ClO_2^-. The oxidation of ACTU involves the successive oxidation of the sulfur center through the sulfenic and sulfinic acids. Oxidation of the sulfinic acid by chlorine dioxide proceeds directly to sulfate bypassing the sulfonic acid. Sulfonic acids are inert to further oxidation and are only oxidized to sulfate via an initial hydrolysis reaction to yield bisulfite, which is then rapidly oxidized. Chlorine dioxide production after the induction period is due to the reaction of the intermediate HOCl species with ClO_2^-. Oligo-oscillatory behavior arises from the fact that reactions that form ClO_2 are comparable in magnitude to those that consume ClO_2, and hence the assertion of each set of reactions is based on availability of reagents that fuel them. A computer simulation study involving 30 elementary and composite reactions gave a good fit to the induction period observed in the formation of chlorine dioxide and in the autocatalytic consumption of ACTU in its oxidation by ClO_2.

Downloaded via CENTERS DISEASE CONTROL & PRVNTN on March 30, 2019 at 18:48:50 (UTC).
See https://pubs.acs.org/sharingguidelines for options on how to legitimately share published articles.

Introduction

The reactivities of most organosulfur compounds involve their oxidations[2] and to some extent their dimerizations.[3] Their oxidations by oxyhalogens have invariably produced nonlinear kinetics. For example, the oxidation of thiourea by bromate is bistable and oscillatory in a flow reactor and displays clock-reaction behavior.[4] The oxidation of thiourea by chlorite generates homoclinic chaos in flow conditions[5] and gives lateral instabilities in unstirred reaction solutions.[6] Most of the recently discovered two-component chemical oscillators involve reactions of oxyhalogen ions and sulfur compounds.[7,8] These oscillators are not as well understood as the pure oxyhalogen versions because very little is known about the kinetics and mechanisms of sulfur-based reactions. The kinetics parameters and mechanistic details of how they react represent the most important data that are needed in order to evaluate plausible mechanisms of sulfur-based chemical oscillators. The study of the kinetics and mechanisms of sulfur-based reactions is, however, complicated by features such as free radical mechanisms,[9−12] polymerizations, autocatalysis,[13] autoinhibition, oligo-oscillations,[14] and variable stoichiometries. In the field of nonlinear chemical dynamics, sulfur compounds are heavily implicated in clock and crazy-clock reactions, chemical waves, and spatial patterns.[15] No complete kinetics study of the oxidation of a sulfur compound has been done so far that does not involve at least one of these nonlinearities.

We recently embarked on a series of studies that involve oxidation (especially S-oxygenation) of a number of organic sulfur compounds.[16] The aim was to derive a generalized algorithm on how the sulfur center can be oxidized from oxidation state −2 to +6. It was important to trap and evaluate the several intermediates that are formed during the course of this oxidation. This would not only help in evaluating the observed nonlinear behavior but would also be helpful in evaluating the varied physiological effects observed with organosulfur compounds, especially thiols[17] and thiocarbamides.[18−20] Our preliminary results have shown us that nearly every organosulfur compound presents a unique reactivity and that no generic oxidation pathway can be derived. Substituted thioureas, for example, appear to deliver vastly differing reaction mechanisms, intermediates, and products even with the same oxidant and under the same reaction conditions. Hydroxymethane-

* To whom correspondence should be addressed. E-mail: rsimoyi@pdx.edu.
† Portland State University.
‡ National Institute for Occupational Safety and Health.

10.1021/jp055805d CCC: $33.50 © 2006 American Chemical Society
Published on Web 02/01/2006

sulfinic acid, for example, can easily be oxidized to a carboxylic acid and sulfate,[21] while its homologue, the biologically important isethionic acid, is extremely inert and is oxidized only by the most powerful oxidizing agents.[22]

We report, in this manuscript, on the oxidation of *N*-acetylthiourea (ACTU) by chlorine dioxide and mildly acidic chlorite. Our previous studies on the oxidation of thiourea by chlorite had shown an extremely versatile reaction that generates a range of nonlinear dynamical behavior that is only rivaled by the venerable Belousov−Zhabotinsky reaction.[23] Although reactions of both thiourea and ACTU by chlorite produced the novel and yet unexplained convective instabilities,[24] the nature and structure of these patterns differed greatly.

Experimental Section

Materials. The following analytical grade chemicals were used without further purification: ACTU, sodium perchlorate (Aldrich), and perchloric acid, 70−72% (Fisher). Commercially available sodium chlorite (Aldrich) varied in purity from 78−88% and was first recrystallized at 50 °C from a 4:6 water−methanol mixture ratio before use. After drying in a vacuum desiccator, this treatment brought the chlorite assay to between 94 and 97%. Analysis of chlorite purity was performed iodometrically by adding acidified iodide and titrating the liberated iodine against standard thiosulfate with starch as indicator.[25,26] Stock chlorite solutions were stabilized by 0.001 M sodium hydroxide since highly acidic environments catalyzed the disproportionation of chlorite solutions to chlorine dioxide and chloride.[27] All chlorite solutions were stored in dark Winchester bottles to reduce exposure to light and were also standardized daily before use. ACTU was assumed to be a good enough standard and was not analyzed nor purified before use.

Tests for Adventitious Metal Ion Catalysis. Water used for preparing reagent solutions was obtained from a Barnstead Sybron Corporation water purification unit capable of producing both distilled and deionized water (Nanopure). Inductively coupled plasma mass spectrometry (ICPMS) was used to quantitatively evaluate the concentrations of a number of metal ions in the water used for our reaction medium. ICPMS analysis showed negligible concentrations of iron, copper, and silver and approximately 1.5 ppb of cadmium and 0.43 ppb in lead as the highest metal ion concentrations. The use of chelators (ethylenediaminetetraacetic acid, deferrioxamine)[28] in reagent waters to sequester these metal ions did not produce significantly different reaction dynamics for all the kinetics data reported in this manuscript.

Methods. Experiments were carried out at 25 ± 0.1 °C. The ionic strength was maintained at 1.0 M ($NaClO_4$). Kinetics runs for rapid oxidations by chlorite were carried out using a Hi-Tech Scientific SF61-DX2 double-mixing stopped-flow spectrophotometer. Chlorine dioxide oxidations were monitored on a Hi-Tech Scientific SF-61AF stopped-flow spectrophotometer with an M300 monochromator and a spectrascan unit. For both stopped-flow ensembles, the data from the photomultipliers were digitized and amplified on an Omega Engineering DAS/50 16-bit A/D board interfaced to Pentium IV computers for storage and analysis. Attempts were also made to use a KinTek Corporation Air Force stopped-flow ensemble, but this instrument gave absorbances and responses that were at variance with the responses obtained from the two Hi-Tech Scientific stopped-flows, and thus the data derived from the KinTek Corporation stopped-flow spectrophotometer were not utilized. The main area of variance was that the Kin-Tek ensemble could not reproduce the "kink" observed, for example, in trace b of Figure 5c. Just as in the two Hi-Tech Scientific stopped-flows, an Applied Photophysics Laboratory MV18 model also reproduced the "kink". Absorbance traces were obtained by following either the appearance or consumption of ClO_2 at 360 nm. ACTU has an isolated absorbance peak in the UV at 267 nm, and thus its consumption could also be monitored spectrophotometrically at 267 nm. We evaluated an absorptivity coefficient of $1.500 \times 10^4\ M^{-1}\ cm^{-1}$ for ACTU at 267 nm. ACTU has another peak at 209 nm, but this peak was not utilized since the product, *N*-acetylurea, also has an appreciable absorbance at this wavelength (see Figure 1S in Supporting Information). Quantitative determinations for sulfate were made using $BaSO_4$ precipitation in the presence of excess oxidant after removing excess chlorite (which could have coprecipitated as $Ba(ClO_2)_2$) by adding excess acidified iodide and evaporating off the iodine formed. The reaction between chlorine dioxide and ACTU is extremely rapid, and thus the stoichiometry of this reaction was determined by simply titrating the oxidant into excess substrate with starch as indicator. Starch prepared with mercuric iodide as a preservative gave a deep blue-black color with excess chlorine dioxide.[29]

Chlorine dioxide was prepared by the standard method of reducing sodium chlorate in a sulfuric acid/oxalic acid mixture.[30] It was also prepared by a novel method discovered in our laboratory of reacting formaldehyde with chlorite.[31] This method relied on the fact that chlorite rapidly oxidized formaldehyde to produce HOCl and formic acid. Further reaction of chlorite and HOCl with formic acid is slow, and hence chlorine dioxide accumulated rapidly and quantitatively from the reaction of (excess) chlorite and HOCl.[32] In both cases, the bubbled air stream loaded with gaseous chlorine dioxide was first passed through a sodium carbonate solution before being collected in ice-cold water at 4 °C at a pH of ∼3.5. Standardization of ClO_2 was also accomplished by iodometric techniques through addition of excess acidified potassium iodide and back-titrating the liberated iodine against standard sodium thiosulfate.[25] The results obtained were confirmed spectrophotometrically by using an absorptivity coefficient for ClO_2 of $1.242\ M^{-1}\ cm^{-1}$ at 360 nm.[33]

A Shimadzu high-performance liquid chromatography (HPLC) system equipped with a SPD6AV UV/Vis detector (Columbia, MD) set at 260 nm and a C18 column (Discovery, 5:m, 25 cm × 4.6 mm, Supelco, Bellefonte, PA) was used for analysis of reaction products. Analytes were eluted from the column using a step linear gradient of 2−40% methanol/water over the first 14 min, followed by a linear gradient increase up to 80% methanol for 18 min.

Stoichiometric Determinations. Reaction mixtures to be used for stoichiometric determinations containing varying ratios of chlorite to ACTU were stored in tightly capped 50-mL volumetric flasks for 24 h before analysis. Each solution was first analyzed for activity in peaks at 209, 267, and 360 nm. The appropriate reaction stoichiometry was attained from a solution in which the peak at 267 nm vanished without the appearance of a peak at 360 nm. This showed that the solution contained just enough chlorite to oxidize ACTU with nothing left over to form chlorine dioxide. This stoichiometry was then confirmed by the aforementioned complementary titrimetric techniques in which excess chlorite was determined iodometrically. By variation of chlorite in excess, a linear relationship was obtained between the thiosulfate titer and amount of excess chlorite. This linear plot was extrapolated to the chlorite concentration axis. The intercept observed is the amount of chlorite needed to just consume ACTU with no excess chlorite

left to oxidize iodide (see Figure 6b). The advantage of this titrimetric method was that the exact strength of the thiosulfate solution was not required for the graphical analysis for as long as the same solution was used throughout.

Results

Product Analysis. This was performed by several complementary techniques. Sulfate was recognized by its precipitate with barium chloride, and chlorine dioxide was characterized by its UV/vis spectrum by a peak at 360 nm. The oxidation of ACTU by chlorite showed a rapid drop in pH that coincided with a sudden formation of chlorine dioxide. Similar results had been obtained in the oxidation of thiourea.[34] The organic residue was determined partly by HPLC. The chlorite−ACTU reaction was quenched at specific times by applying the reaction mixture to a 100 mg C18 solid phase extraction column, washing it with water, and eluting off the products with methanol. The parent ACTU compound was oxidized very quickly, in fact, within the time it took to pipet the reaction mixture into the column (see Figure 5a, for example, in which ACTU consumption is complete in less than 10 s.). The major oxidation product was noted at 14.8 min. This peak continued to increase up to 30 min of reaction time. Up to three other oxidation products which also increased with time were noted with the predominant one at 12.5 min and another at 17.14 min. After 24 h, the major peak was noted at 14.27 min, which we assumed to be just a shift of the 14.8-min peak. It was evident that there are at least 2 and at most 3 intermediate products that appear very quickly but are later consumed to form the predominant product at 14.27 min. This is in line with our previous assertions that the oxidation pathway of thiocarbamides proceeds through the formation of a series of oxo-acids: sulfenic, sulfinic, and sulfonic before cleaving the C−S bond to form sulfate and a urea-based compound.[35]

Stoichiometry. The stoichiometry of the chlorite−ACTU reaction was experimentally determined as

$$2ClO_2^- + CH_3CONH(NH_2)C{=}S + H_2O \rightarrow CH_3CONH(NH_2)C{=}O + SO_4^{2-} + 2Cl^- + 2H^+ \quad (R1)$$

This stoichiometry was deduced as the highest chlorite to ACTU ratio that could be used without the production of chlorine dioxide after an incubation period of more than 24 h. This ratio was later reconfirmed by titrimetric techniques. The yield percentage of sulfate ($BaSO_4$ precipitation), at 97%, was within the limits of a 1:1 ratio of ACTU to sulfate. The 2:1 stoichiometric ratio also confirmed that the sulfur center is oxidized from oxidation state −2 to +6 (sulfate). The stoichiometry of the chlorine dioxide−ACTU was determined as

$$8ClO_2(aq) + 5CH_3CONH(NH_2)C{=}S + 9H_2O \rightarrow 5CH_3CONH(NH_2)C{=}O + 5SO_4^{2-} + 8Cl^- + 18H^+ \quad (R2)$$

The 8:5 ratio was obtained from both simple titrimetric techniques and by following the chlorine dioxide absorbance

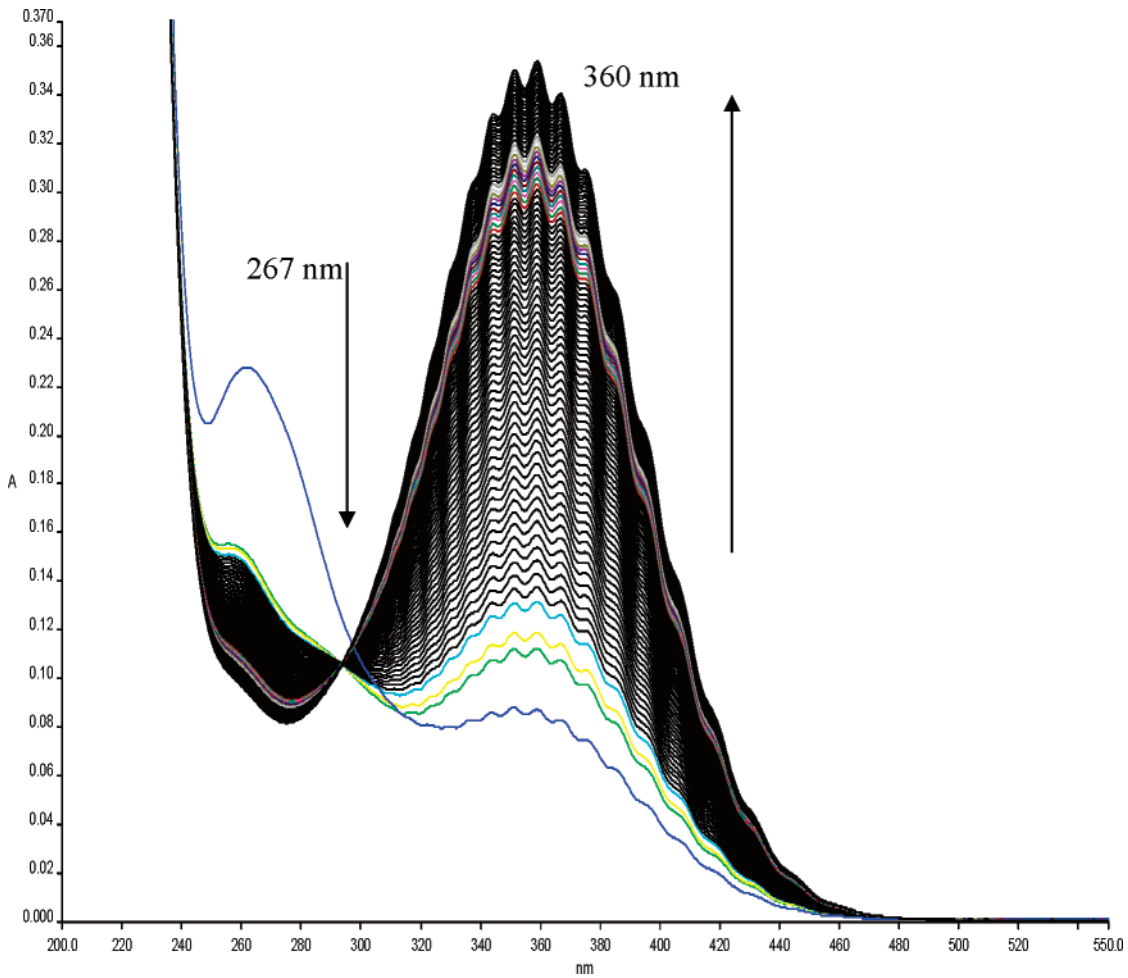

Figure 1. (a) Spectral scan measurements of the reaction of ACTU and chlorite taken every 35 s with no acid added. (b) Peak of ACTU at 267 nm being consumed and formation of chlorine dioxide at 360 nm with no noticeable formation of any intermediate. [ACTU] = 1.0×10^{-3} M, [ClO_2^-] = 3.0×10^{-3} M.

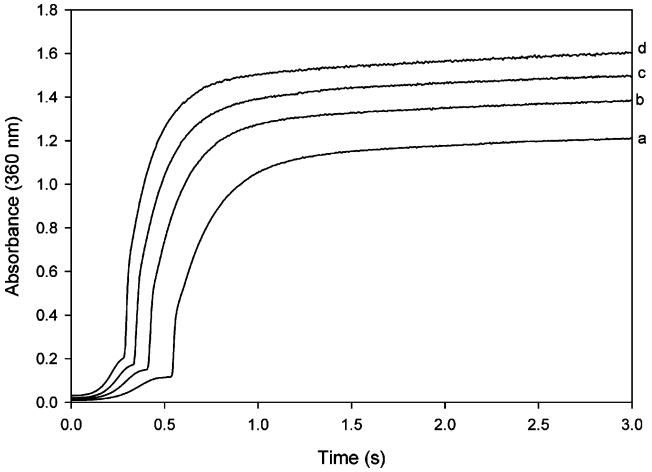

Figure 2. The effect of varying chlorite in the oxidation of ACTU using chlorite as the oxidant. The rate of formation of chlorine dioxide was gentle and gradual at the initial part of the plot, followed by a rapid increase in the formation of chlorine dioxide at 360 nm. As the concentration of chlorite increases formation of chlorine dioxide also increases. [ACTU] = 2.5×10^{-3} M, [$HClO_4$] = 2.0×10^{-2} M, l $_{NaClO4}$ = 1 M. [ClO_2^-] = (a) 2.4×10^{-2} M, (b) 3.0×10^{-2} M, (c) 3.6×10^{-2} M, (d) 4.2×10^{-2} M.

peak at 360 nm. Since there was no interference from the organic reactants and residues, at this peak, absorbance noted here could be attributed solely to chlorine dioxide. The 8:5 ratio was also conclusively deduced from the data shown in parts a and b of Figure 6. In this series of experiments, excess ClO_2 was maintained in all the reaction solutions. At the end of the reaction, the remaining ClO_2 was noted. Figure 6b shows a plot of final absorbance (from excess ClO_2). This plot is linear, with an intercept on the $[ClO_2]_0$ axis of 2.0×10^{-4} M ClO_2. This is the ClO_2 concentration needed to just completely oxidize ACTU with no ClO_2 left to absorb at 360 nm. Since a constant 1.25×10^{-4} M ACTU was used for this series of experiments, an 8:5 ratio for stoichiometry R2 could be deduced.

Reaction Kinetics. The reaction is very fast, and the rapid-scan traces in Figure 1 show a rapid decay of the peak at 267 nm within the first 30 s of the reaction. However during this initial rapid consumption of ACTU, no activity is observed at the 360-nm peak (which would have indicated formation of chlorine dioxide). When the absorbance at 267 nm has decayed substantially, the peak at 360 nm starts to grow. This sequence is extremely important in trying to obtain a plausible mechanism for the oxidation of ACTU. Figure 2 shows absorbance traces at a single wavelength (360 nm) of what the rapid scans in Figure 1 show between 200 and 450 nm. At 360 nm, there is a short induction period with very slow to negligible formation of chlorine dioxide that plateaus out before rapid ClO_2 formation commences. Chlorite visibly reduces the induction period but does not affect the rate of formation of chlorine dioxide at the end of this induction period. There is a linear relationship between the inverse of the induction period and initial chlorite concentrations, but at high chlorite concentrations this linearity is lost. Higher chlorite concentrations seem to inordinately reduce the induction period, suggesting the possibility of autocatalytic formation of some of the reactive intermediates derived from chlorite.

Parts a and b of Figure 3 show that the effect of acid is dependent on its strength. Data in Figure 3a were taken at low acid concentrations with a pH $\approx$ pK_a of chlorous acid,[36] $HClO_2$. In these pH conditions, chlorine(III) species exist in the reaction medium in both the protonated, $HClO_2$, and unprotonated,

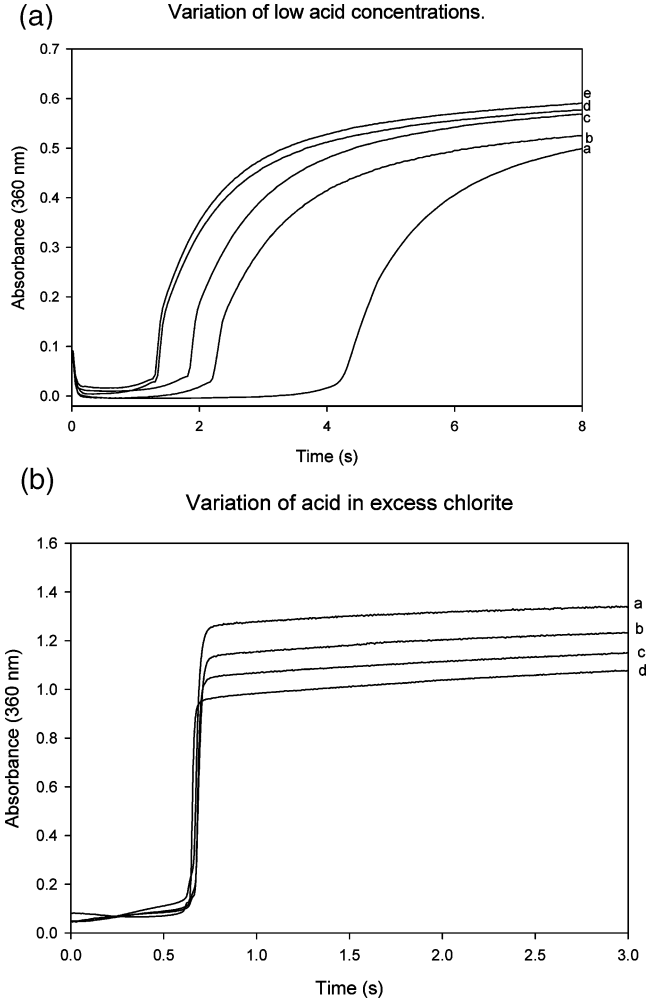

Figure 3. (a) Effect of acid at low acid concentrations in which pH > pK_a of $HClO_2$. Increasing acid concentrations decreases the induction period and increases the rate of formation of chlorine dioxide. A linear relationship exists between the inverse of the induction period and acid concentrations, but this effect soon saturates as acid is increased past 7.5×10^{-4} M. [ACTU] = 2.5×10^{-3} M, [ClO_2^-] = 1.2×10^{-2} M, l $_{NaClO4}$ = 1 M. [$HClO_4$] = (a) 2.5×10^{-4} M, (b) 5.0×10^{-4} M, (c) 7.5×10^{-4} M, (d) 1.0×10^{-3} M, (e) 1.25×10^{-3} M. (b) The effect of high acid concentrations on the oxidation of ACTU by chlorite.The induction period before the formation of chlorine dioxide at 360 nm is invariant as acid concentrations increases, but the amount of chlorine dioxide formed decreases with increases in acid concentrations. Acid can be said to be inhibiting the formation of chlorine dioxide. [ACTU] = 2.5×10^{-3} M, [ClO_2^-] = 3.0×10^{-2} M, l $_{NaClO4}$ = 1 M. [$HClO_4$] = (a) 2.5×10^{-1} M, (b) 3.75×10^{-1} M, (c) 5.0×10^{-1} M, (d) 6.25×10^{-1} M.

ClO_2^-, forms. At low acid concentrations, pH > pK_a, acid shortens the induction period (Figure 3a), and in this case higher acid concentrations delivered higher rates of formation of chlorine dioxide. The acid concentrations used to generate the data in Figure 3a were deliberately taken in the range 2.5×10^{-4} to 1.25×10^{-3} M because this range induces measurable changes in $HClO_2$ and ClO_2^- concentrations. Figure 3b shows the response of the induction period to a higher range of acid concentrations to those shown in Figure 3a. These higher acid concentrations delivered a response in which the induction period was shorter and invariant to changes in acid concentrations. The amount of chlorine dioxide formed after the induction period in Figure 3b was stunted by higher acid concentrations. This was the exact opposite to that obtained from Figure 3a. Figure 4 shows complex and oligo-oscillatory[37] formation of

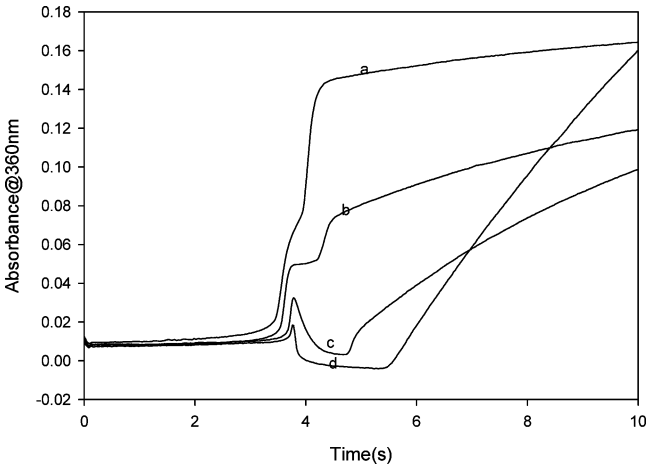

Figure 4. Oligo-oscillatory formation of chlorine dioxide at stoichiometric excess of chlorite concentrations. Trace a, with a high oxidant-to-reductant ratio of 10, shows a monotonic increase in chlorine dioxide. Lower ratios show a discontinuity in chlorine dioxide which finally culminates in transient formation of chlorine dioxide. $[ClO_2^-] = 5.0 \times 10^{-3}$ M, $[HClO_4] = 2.5 \times 10^{-1}$ M, $l_{NaClO4} = 1$ M. [ACTU] = (a) 5.0×10^{-4} M, (b) 1.0×10^{-3} M, (c) 1.5×10^{-3} M, (d) 2.0×10^{-3} M.

ClO_2 at varying oxidant-to-reductant ratios. These oligo-oscillatory dynamics are pertinent only at the acid concentrations involved. A change in acid concentrations resulted in the formation of oligo-oscillatory behavior at different oxidant-to-reductant ratios. As will be noted later in the discussion, higher acid concentrations stabilize some of the oxo-acid intermediates,[38] thereby allowing accumulation and consumption of ClO_2 to occur before these intermediates have been completely oxidized.

The chlorite−ACTU reaction, when monitored at 267 nm, shows strongly sigmoidal decay kinetics in the depletion of ACTU. Figure 5a shows a series of experiments performed in excess ClO_2^- conditions. The data shows the typical sigmoidal decay kinetics that denotes autocatalysis with a constantly increasing rate of consumption of ACTU. Higher chlorite concentrations deliver much more rapid autocatalytic rates of consumption of the substrate. The different initial absorbances observed in this figure are derived from contribution from initial chlorite concentrations. This contribution is also reflected in the final absorbances observed after all the ACTU has been consumed. Data shown in Figure 5a (as well as Figure 5b) show an abrupt end of the autocatalytic sigmoidal behavior, which is followed by normal decay kinetics near the end of the reaction. Figure 5b shows the inhibitory effect of acid on the reaction, which mirrors the data shown in Figure 3b. Lower acid concentrations (data not shown) catalyze the rate of disappearance of ACTU. When pH ≤ pK_a, however, acid retards the autocatalytic consumption of ACTU. Upon varying ACTU concentrations, sigmoidal kinetics are preserved at the various oxidant-to-reductant ratios, with the reaction time increasing with increase in ACTU concentrations for fixed chlorite concentrations. This is expected if ACTU is not an autocatalytic species. Figure 5c shows a superimposition of these two sets of data (at 267 and 390 nm). There is a very strong correlation between these events. With the high absorptivity coefficient for ACTU at 267 nm, it was not possible to utilize exactly the same conditions as those in Figures 2−4. The low concentrations of ACTU used in parts a and b of Figure 5 were insufficient to show measurable ClO_2 absorbances at 360 nm without greatly magnifying these absorbance changes observed at 360 nm (Figure 5c, trace c magnified from trace a). Figure 5c shows

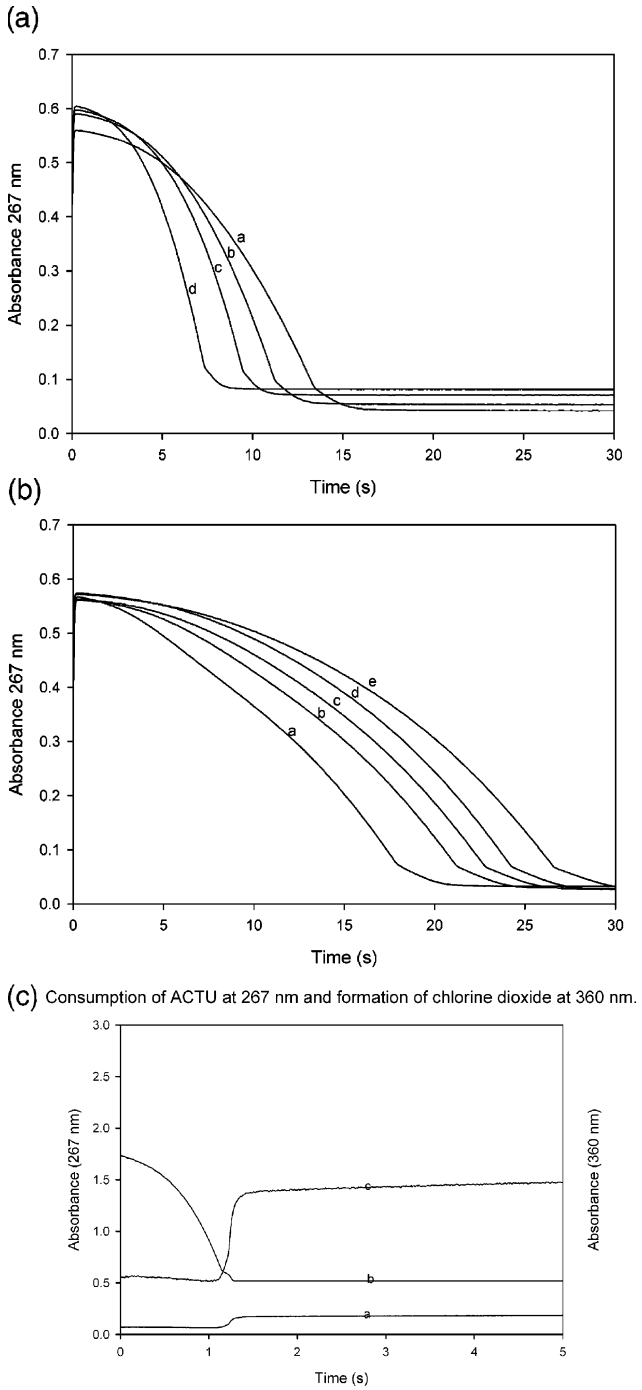

Figure 5. (a) The chlorite−ACTU reaction observed at 267 nm. Decay kinetics show simple sigmoidal kinetics. [ACTU] = 4.0×10^{-5} M, $[HClO_4] = 2.5 \times 10^{-2}$ M, $l_{NaClO4} = 1$ M. $[ClO_2^-]$ = (a) 7.5×10^{-4} M, (b) 1.0×10^{-3} M, (c) 1.25×10^{-3} M, (d) 1.5×10^{-3} M. (b) Combination of absorbance traces taken at 360 and 267 nm for the same initial conditions. Chlorine dioxide formation commences after most of the ACTU has been oxidized. (c) Trace a magnified 8×. $[ACTU]_0 = 1.25 \times 10^{-4}$ M, $[ClO_2^-] = 1.5 \times 10^{-2}$ M, $[HClO_4]_0 = 5.0 \times 10^{-1}$ M, $l_{NaClO4} = 1$ M.

that, at 0.50 M acid, the start of the formation of chlorine dioxide coincides with the end of the sigmoidal consumption kinetics of ACTU. What appears as an induction period at 360 nm is actually an autocatalytic regime at 267 nm in which the substrate is rapidly oxidized.

Direct ClO_2(aq)−ACTU Reaction. This reaction could also be monitored at both 267 nm and at 360 nm. It is a very rapid reaction that occurs on a faster time scale when compared to

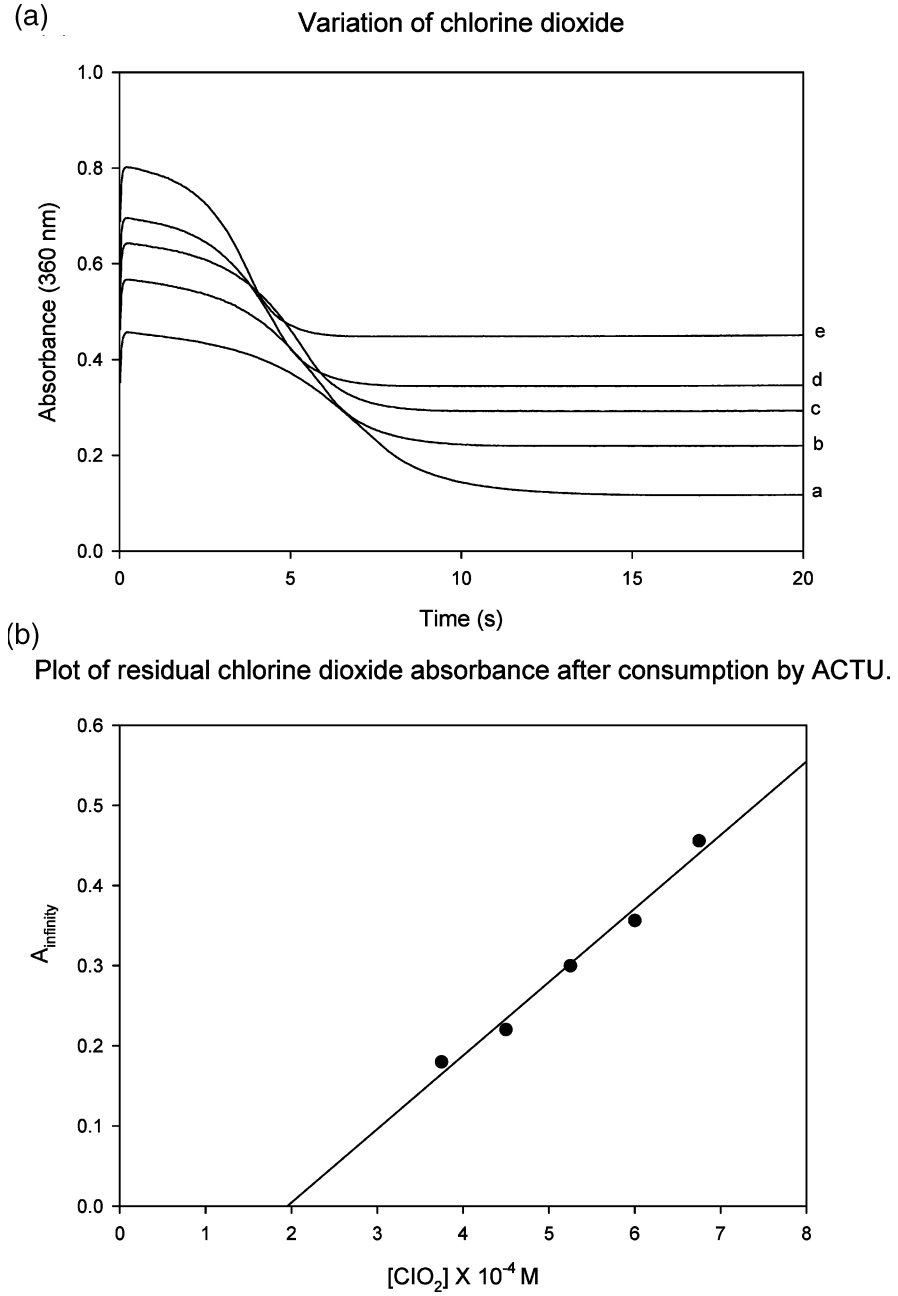

Figure 6. (a) Effect of varying chlorine dioxide at 360 nm in the oxidation of ACTU. Sigmoidal kinetics persists throughout with the rate of depletion of chlorine dioxide rapidly enhanced by ACTU. Consumptions of chlorine dioxide are over in 10 s. In all traces shown, the oxidant (ClO_2(aq)) is in excess. $[ACTU]_0 = 1.25 \times 10^{-4}$ M, $[HClO_4]_0 = 2.5 \times 10^{-1}$ M, $l_{NaClO4} = 1$ M. $[ClO_2(aq)]_0 =$ (a) 3.75×10^{-4} M, (b) 4.5×10^{-4} M, (c) 5.25×10^{-4} M, (d) 6.0×10^{-4} M, (e) 6.75×10^{-4} M. (b) Plot of residual chlorine dioxide absorbance after consumption by ACTU. This confirms the stoichiometry of the reaction of ACTU in excess chlorine dioxide. $[ACTU]_0 = 1.25 \times 10^{-4}$ M, $[HClO_4]_0 = 2.5 \times 10^{-1}$ M, $l_{NaClO4} =$ 1 M. $[ClO_2(aq)]_0 =$ (a) 3.75×10^{-4} M, (b) 4.5×10^{-4} M, (c) 5.25×10^{-4} M, (d) 6.0×10^{-4} M, (e) 6.75×10^{-4} M.

the chlorite−ACTU (see Figure 8a). Increasing chlorine dioxide concentrations increased the rate of consumption of ACTU (see Figure 6a). Data shown in Figure 6a were acquired with excess oxidant such that the reaction's end products contained some chlorine dioxide with no ACTU. This explains the different final absorbances observed for each experiment. From these types of experiments, one could evaluate the stoichiometry of the ClO_2−ACTU reaction, which concurred with the one obtained by titration in stoichiometry R2 (see the Results section). Figure 6b, as noted in the Results section, shows a plot of the residual ClO_2 absorbance after full consumption of ACTU. The plot is linear and shows that 1.25×10^{-4} M ACTU requires 2.0×10^{-4} M of ClO_2 for a reaction mixture that just completely consumes ACTU. This confirmed the 8:5 stoichiometry of ClO_2:ACTU.

Despite the very high oxidant-to-reductant ratios used in Figure 7 of over 10:1, no pseudo-first-order kinetics are observed in the consumption of ACTU. The reaction is essentially over in less than 2 s. In unbuffered conditions, and at low acid concentrations, the reaction is over in about a tenth of a second. Acid shows a very strong retarding effect on the rate of reaction over a wide range of acid concentrations, which is in contrast to the comparable chlorite oxidation kinetics in which acid effects depend on the acid strength. The decay kinetics displayed in Figure 7, however, could be altered to the standard (monotonic) concave-shaped decay kinetics by the use of high acid

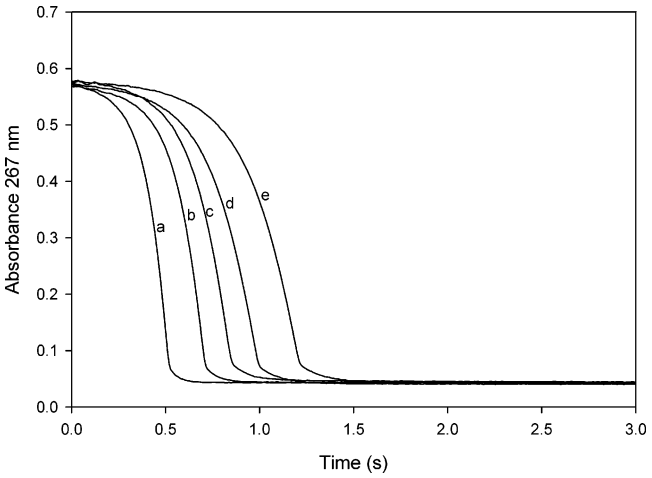

Figure 7. Chlorine dioxide oxidation. Inhibitory effect of medium acid concentration changes on the oxidation of ACTU by chlorine dioxide. $[ACTU]_0 = 4.0 \times 10^{-5}$ M, $[ClO_2]_0 = 4.95 \times 10^{-4}$ M, $l_{NaClO4} = 1$ M. $[HClO_4]_0$ = (a) 1.0×10^{-2} M, (b) 1.5×10^{-2} M, (c) 2.0×10^{-2} M, (d) 2.5×10^{-2} M, (e) 3.0×10^{-2} M.

concentrations and concomitantly with $[ACTU]_0 \gg [ClO_2]_0$. Such experimental traces were performed at 1.0 M $HClO_4$ and with $40 > [ACTU]_0/[ClO_2]_0 > 30$. Pseudo-first-order kinetics were observed for 70% of the reactions, which show that the reaction of chlorine dioxide and ACTU is first order in ClO_2. These data are shown as Supporting Information parts a−c of Figures 3S.

Comparative Kinetics. Figure 8a shows two traces taken with exactly the same conditions except that one has 4.95×10^{-4} M ClO_2 and the other has 4.95×10^{-4} M ClO_2^-. This figure shows that chlorine dioxide oxidations occur at a much more rapid rate than comparable chlorite oxidations. We also ran comparison traces of oxidation rates of thiourea and ACTU to evaluate the effect of the addition of the *N*-acetyl group. The data obtained showed that addition of the *N*-acetyl group radically alters the reaction kinetics. At 0.063 M acid and 0.0007 M ClO_2, the oxidation of ACTU is over in about 0.5 s, while that of unsubstituted thiourea is considerably slower at 1.5 s and with milder autocatalysis (see Supporting Information Figure 4S(a). Chlorite shows a mild catalytic effect on chlorine dioxide oxidations which would have been expected from the addition of the ClO_2^-/ACTU reaction to the ClO_2/ACTU reaction (Supporting Information Figure 4Sb). The parallel nature of the absorbance traces shows that chlorite is not an autocatalytic species in this reaction. Several chlorite oxidation studies have implicated HOCl as the most important oxidizing species. The HOCl−ACTU reaction was easier to follow at the absorption peak of HOCl of 234 nm. HOCl was obtained by bubbling chlorine gas into water, adjusting the pH and standardizing the solution iodometrically. This reaction is so fast that its rate is beyond the capabilities of the Hi-Tech Scientific 61AF spectrophotometer. It is essentially over within the mixing time of the reaction (Supporting Information Figure 4Sc). The oxidation of an organosulfur compound (such as ACTU) is postulated to proceed through a number of sulfur oxo-acid intermediates.[34] We attempted to synthesize the sulfinic and sulfonic acid intermediates of ACTU with no success. We, however, managed to synthesize the sulfonic acid of dimethylthiourea (dimethylaminoiminomethanesulfonic acid, $HMeN(MeNd)C-SO_3H$, (DMAIMSOA) whose kinetics of oxidation we could examine and approximate to those of the sulfonic acid of ACTU. We also found commercially available cysteinesulfinic acid[39] as well as formamidinesulfinic acid. Figure 8b shows that, while the ClO_2 oxidations of the sulfinic acids are fast, the oxidation of sulfonic acids such as DMAIMSOA is very slow, to the point of being inert to chlorine dioxide. The inertness of the sulfonic acid to both ClO_2 and ClO_2^- is useful in explaining the nonlinear kinetics observed in the formation of ClO_2 in ClO_2^-/ACTU reactions.

Mechanism

Three major reactions exist in the ClO_2^-−ACTU reaction mixture. The first reaction consumes ACTU, the second forms chlorine dioxide, and the third involves the reaction between ACTU and its metabolites with chlorine dioxide. The mechanism of the formation of chlorine dioxide from the interactions between oxychlorine species is well known.[40,41] This manuscript will deal with the mechanism of the first and last reactions.

Consumption of ACTU. Parts a and b of Figure 5 clearly show the autocatalytic consumption of ACTU. This autocatalysis involves the formation of some intermediate oxychlorine species, which is more reactive than the parent chlorite. Oxidation of thiol groups can proceed via the formation thiyl radicals[11,42,43] or through S-oxygenation processes that form successively sulfenic, sulfinic, and sulfonic acids.[2,44−46] Thiyl radical formation is mediated by one-electron metal ions that catalyze their initial formation.[11] Our reagent solutions contain negligible concentrations of metal ions based on our ICPMS analysis. The oxidation of ACTU by chlorite should thus proceed predominantly via the sulfur oxo-acids route. Successive S-oxygenation processes involve two-electron transfers from a chlorine center to a sulfur center. The only reactive species that can be derived from chlorite reductions are hypochlorous acid and aqueous chlorine. Any two-electron reduction of chlorite should produce HOCl

$$ClO_2^- + 3H^+ + 2e^- \rightarrow HOCl + H_2O \qquad (R3)$$

Chlorine can be formed from its reverse hydrolysis reaction[47]

$$HOCl + Cl^- + H^+ \rightarrow Cl_2(aq) + H_2O \qquad (R4)$$

Since chloride is a product of the reduction of chlorite and Cl_2 is subsequently formed from HOCl, if the rate of oxidation of ACTU by HOCl is very fast, then oxidation by Cl_2 will not be a significant pathway. Furthermore, if both HOCl and Cl_2 are strong oxidants, then their reactions will be kinetically indistinguishable if one is observing reaction rate through consumption of ACTU. The two-electron oxidation of ACTU by chlorite (reaction R5) should give the unstable sulfenic acid[13,34,48]

$$ClO_2^- + CH_3CONH(NH_2)C{=}S \rightarrow CH_3CON{=}(NH_2)CSOH + OCl^-;\ k_1 \qquad (R5)$$

$$OCl^- + H^+ \rightleftharpoons HOCl \qquad (R6)$$

Reaction R6 is a rapid protolytic reaction that can be combined with reaction R5 for a composite termolecular reaction. The formation of the reactive species, HOCl, will introduce the oxyhalogen reaction which produces ClO_2

$$2ClO_2^- + HOCl + H^+ \rightarrow 2ClO_2 + Cl^- + H_2O \qquad (R7)$$

Reaction R7 has been extensively studied[32,49] and is known to be a rapid reaction that is catalyzed by acid. Reaction R7 will compete with any other reactions that consume HOCl. These are the reactions that involve the oxidation of

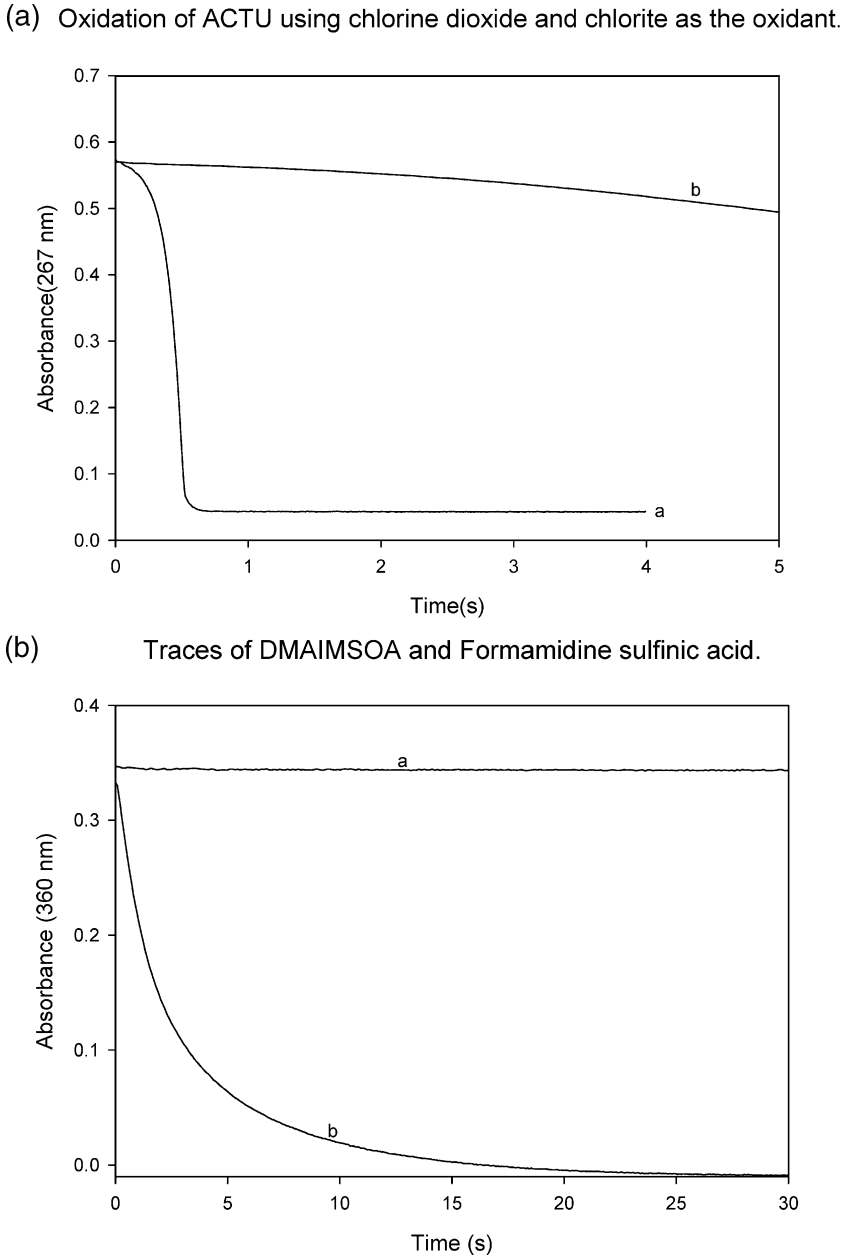

Figure 8. (a) Superimposed absorbance traces comparing the oxidation rates of ClO_2^- and ClO_2. Both chlorite and chlorine dioxide are maintained at 4.95×10^{-4} M with $[ACTU]_0 = 4.0 \times 10^{-5}$ M and $[HClO_4]_0 = 1.0 \times 10^{-2}$ M. The chlorine dioxide oxidation is over in less than a second while the chlorite oxidation took over 35 s. (b) Comparison of the rates of oxidation of a typical aminosulfinic acid (aminoiminomethanesulfinic acid, AIMSA) and a typical aminosulfonic acid (dimethylaminoiminomethanesulfonic acid, DMAIMSOA) by chlorine dioxide. The sulfinic acids are readily oxidized while the sulfonic acids are effectively inert to further oxidation in acidic media. Both traces had 0.125 M perchloric acid. (a) $[DMAIMSOA]_0 = 4.0 \times 10^{-2}$ M, $[ClO_2]_0 = 2.70 \times 10^{-4}$ M, (b) $[AIMSA]_0 = 4.0 \times 10^{-4}$ M, $[ClO_2]_0 = 2.58 \times 10^{-4}$ M.

ACTU and its intermediate oxo-acids

$$HOCl + CH_3CONH(NH_2)C{=}S \rightarrow CH_3CON{=}(NH_2)CSOH + Cl^- + H^+ \quad (R8)$$

$$HOCl + CH_3CON{=}(NH_2)CSOH \rightarrow CH_3CON{=}(NH_2)CSO_2H + Cl^- + H^+ \quad (R9)$$

$$HOCl + CH_3CON{=}(NH_2)CSO_2H \rightarrow CH_3CON{=}(NH_2)CSO_3H + Cl^- + H^+ \quad (R10)$$

$$HOCl + CH_3CON{=}(NH_2)CSO_3H + H_2O \rightarrow CH_3CONH(NH_2)C{=}O + SO_4^{2-} + Cl^- + 3H^+ \quad (R11)$$

where $CH_3CON{=}(NH_2)CSO_2H$ is the sulfinic acid, $CH_3CON{=}(NH_2)CSO_3H$ the sulfonic acid, and $CH_3CONH(NH_2)C{=}O$ is *N*-acetylurea, the final oxidation product. The global reaction dynamics, when observed through absorbance traces at 360 nm, will be determined by the relative rates of reaction R7 and reactions R8−R11. If reaction R7 is much faster than reactions R8−R11, and oxidations of the organosulfur set of compounds by chlorine dioxide are slow, then an almost instant formation of chlorine dioxide will be observed with no discernible induction period.[31] Since we observe a finite induction period and oligo-oscillatory dynamics for the reaction (see Figure 4), this suggests that, for awhile into the reaction, reactions R8−R11 will be dominant. This is especially so at the beginning of the reaction where reaction R8 will be dominant due to the abundance of reductant. On the basis of the instability of the sulfenic acid, we expect reaction R9 to be as rapid or faster

than R8. The rate-determining step for the oxidation of ACTU would be reactions of type R5. The sulfenic acid's instability introduces its possible disproportionation (R12) as well as its dimerization (R13)[50−52]

$$2CH_3CON{=}(NH_2)CSOH \rightarrow CH_3CONH(NH_2)C{=}S + CH_3CON{=}(NH_2)CSO_2H \quad (R12)$$

$$CH_3CON{=}(NH_2)CSOH + CH_3CONH(NH_2)C{=}S \rightarrow [CH_3CON{=}(NH_2)C{-}S{-}]_2 + H_2O \quad (R13)$$

However, in the presence of excess oxidant, reactions R12 and R13 will be stunted and should not be significant since the products of R12 and R13 will still be susceptible to further oxidation. [As long as further oxidations (reactions R9 and R10) as well as the oxidation of the dimer are facile,[53] then reactions R12 and R13 will be kinetically inconsequential.] Reactions R12 and R13 will be important in conditions where there is excess reductant because the preferred oxo-acid intermediates of ACTU would be the sulfinic and sulfonic acids as well as the dimeric formamidine-type species. We could not synthesize the dimer of ACTU, but the dimer of thiourea, formamidine disulfide ($H_2N(=NH)CS-)_2$, is commercially available. Both thiourea and formamidine disulfide were oxidized by chlorine dioxide. The reaction of formamidine disulfide with chlorine dioxide, however, was found to be faster than the oxidation of thiourea by chlorine dioxide (see Supporting Information Figure 5S). Thus, in the presence of excess oxidant, reaction R13 would not affect the overall global reaction dynamics with respect to rate of consumption of ACTU.

Sigmoidal Kinetics. In a publication from 1949, Taube and Dodgen[54] used isotopic labeling to prove that reaction R7 proceeds through an asymmetric intermediate, Cl_2O_2

$$ClO_2^- + HOCl + H^+ \rightleftharpoons Cl_2O_2 + H_2O \quad (R14)$$

Any further 2-electron reduction of this intermediate will produce 2 HOCl molecules

$$Cl_2O_2 + 2H^+ + 2e^- \rightarrow 2HOCl \quad (R15)$$

Addition of reaction R14 and R15 will show quadratic autocatalysis in production of HOCl

$$ClO_2^- + HOCl + 3H^+ + 2e^- \rightarrow 2HOCl + H_2O \quad (R16)$$

If reactions R8−R11 are fast, and one can assume that the two electrons in reaction R15 can be derived from ACTU or any of its intermediates that are not yet oxidatively saturated, then quadratic autocatalysis will be observed, with HOCl as the autocatalytic species.[55,56] The only important prerequisite will be that reactions of type R15 should be faster than the R8−R11 group.

Acid Dependence. Figure 3a shows the catalytic effect of acid (at low acid concentrations) by the fact that higher acid concentrations decreased the induction period. Figure 5b, however, also shows that the rate of consumption of ACTU is retarded by acid when pH $\approx$ pK_a($HClO_2$). Two protolytic equilibria exist in the reaction mixture

$$ClO_2^- + H^+ \rightleftharpoons HClO_2;\ K_a^{-1} \quad (R17)$$

$$CH_3CONH(NH_2)C{=}S + H^+ \rightleftharpoons [CH_3CONH(NH_2)C{-}SH]^+;\ K_b \quad (R18)$$

The study of the protonation of thiourea showed that, even though both the N and S centers are both basic, the first proton attaching to thiourea in acidic environments oscillates between these two centers while spending more time on the sulfur center.[52] The protonation of the amino groups, though feasible, has no consequence on the reactivity of this molecule. They (amino groups) are also located distal to the reactive thiol group. No reactivity has been observed on the N−C−N moiety of ACTU as this is retained intact in the product *N*-acetylurea. It is worth noting that the value of K_b in reaction R18 has no thermodynamic significance. Its value, kinetically, is to quantify acid retardation within a specific range of acid concentrations. Highly acidic environments will produce the unfavorable initiation reaction of chlorous acid with protonated ACTU (reaction R21) and lower acid conditions will introduce reaction R5. The protonation of ACTU can be visualized by the following scheme

Thiourea Protonation Scheme

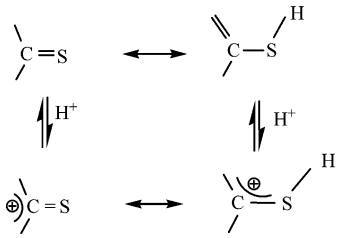

The protonation of the keto and enol forms of thiocarbamides will give different tautomeric forms of the protonated molecule. The form with the charge delocalized between the N and S centers will reduce the nucleophilicity of the S center.

The ideal situation for the fastest initiation reaction (R5 type of reactions) would involve the protonated thiol $[CH_3CONH(NH_2)C{-}SH]^+$ with unprotonated Cl(III) species

$$ClO_2^- + [CH_3CONH(NH_2)C{-}SH]^+ \rightarrow CH_3CON{=}(NH_2)CSOH + HOCl;\ k_2 \quad (R19)$$

Reaction R19, however, is an unlikely combination, given that pK_a of chlorous acid is 1.72.[49,57] Low pH conditions will have negligible concentrations of ClO_2^- and high pH conditions have negligible concentrations of protonated ACTU. There are two other initiation reactions that are dependent on acid concentrations, R20 and R21

$$HClO_2 + CH_3CONH(NH_2)C{=}S \rightarrow CH_3CON{=}(NH_2)CSOH + HOCl;\ k_3 \quad (R20)$$

$$HClO_2 + [CH_3CONH(NH_2)C{-}SH]^+ \rightarrow CH_3CON{=}(NH_2)CSOH + HOCl + H^+;\ k_4 \quad (R21)$$

The experimentally observed acid dependence can now be explained by each of the four reactions, R5, R19, R20, and R21, will be dominant at each specific acid concentration. For example, at pH conditions around 3, only reactions R5 and R20 will be relevant, meaning the observed acid catalysis must arise from the fact that $k_3 > k_1$. Acid catalyzes the reaction (reduced induction periods and increased rate of consumption of ACTU) as acid concentrations are increased until the pK_a of $HClO_2$ is reached. The rate of reaction, on the basis of rate of consumption of ACTU as pH is lowered toward the pK_a of $HClO_2$ is given by

$$\frac{-\mathrm{d[ACTU]}}{\mathrm{d}t} = \frac{[\mathrm{ACTU}]_0[\mathrm{Cl(III)}]_\mathrm{T}}{1 + K_\mathrm{a}[\mathrm{H}^+]}(k_1 + k_3K_\mathrm{a}[\mathrm{H}^+]) \quad (1)$$

where $[\mathrm{Cl(III)}]_\mathrm{T}$ is the sum of $[\mathrm{ClO_2}^-]$ and $[\mathrm{HClO_2}]$. At low acid concentrations, the term in the denominator approximates to unity and rate of reaction will increase with acid for as long as $k_3 > k_1$. Data in Figures 3a are supported by eq 1. At pH $K_\mathrm{a}(\mathrm{HClO_2})$, then $[\mathrm{Cl(III)}]_\mathrm{T} = [\mathrm{HClO_2}]$ with diminishing $\mathrm{ClO_2}^-$ concentrations. After the reaction medium saturates with chlorous acid, the initial rate of reaction becomes

$$\frac{-\mathrm{d[ACTU]}}{\mathrm{d}t} = \frac{\mathrm{d[HOCl]}}{[\mathrm{d}t]} = (k_3[\mathrm{ACTU}]_0[\mathrm{Cl(III)}]_\mathrm{T}) \quad (2)$$

Further decrease in pH, however, introduces the "protonation" equilibrium of ACTU with dominant initiation reactions now being R20 and R21 with new rate of reaction becoming

$$\frac{-\mathrm{d[ACTU]}}{\mathrm{d}t} = \frac{\mathrm{d[HOCl]}}{\mathrm{d}t} = \frac{[\mathrm{ACTU}]_\mathrm{T}[\mathrm{Cl(III)}]_\mathrm{T}}{1 + K_\mathrm{b}[\mathrm{H}^+]}(k_3 + k_4[\mathrm{H}^+]) \quad (3)$$

$[\mathrm{ACTU}]_\mathrm{T}$ is the sum of the "protonated" and "unprotonated" ACTU. In eq 3, $k_3 > k_4$ and hence further increases in acid will result in a retardation in the rate of reaction as has been observed in data shown in Figure 5b. The rationalization of the acid dependence data involves the successive application of rate eqs 1, 2 and 3 as acid concentrations are increased. This series of equations will predict a bifurcation of acid dependence that starts with catalysis, then saturation, and finally retardation as has been experimentally observed. Nonlinearity of the reaction system in the form of autocatalysis reduces the relevance of reactions R5, R19, and R20 to the initial stages of the reaction only as autocatalysis will take over just after initiation of the reaction. Attempts to experimentally derive kinetics constants k_1, k_3, and k_4 were unsuccessful due to the sigmoidal nature of the kinetics. Approximate values were derived from computer simulations of the overall reaction dynamics. A schematic representation of reaction R20 is shown in Scheme 1.

Chlorite is more basic than the thiocarbamide and will be protonated first before ACTU is protonated as the acid concentrations are slowly increased. Scheme 1 will be relevant between pH 5 and 2. Steps A and B will be rapid and reversible, and the rate-determining step will be the cleavage of the S−Cl bond in C to release HOCl and the unstable sulfenic acid. Higher acid conditions will reduce the nucleophilicity of the thiol group and shift equilibrium of step A to the left, thereby retarding the reaction.

Chlorine Dioxide−ACTU Reaction. Data in parts a and b of Figure 6 and Figure 7 show that the direct reaction between chlorine dioxide and the substrate is directly proportional to concentrations of both reagents. At high $[\mathrm{ClO_2}]_0$ to $[\mathrm{ACTU}]_0$ ratios and at low acid concentrations the reaction is so rapid that it is essentially complete within 0.1 s. Figure 7, however, shows an acid retardation. Protolytic equilibria R17 and R18 can also be utilized to explain the acid retardation since most oxyhalogen-based reactions are known to be acid catalyzed. In most chlorine dioxide oxidations, the first step is the addition of an electron on the odd-electron deficient chlorine center to form the more stable Cl(III) species, chlorite[58]

$$\mathrm{ClO_2} + \mathrm{e}^- \rightarrow \mathrm{ClO_2}^-;\ E_0 = 0.94\ \mathrm{V} \quad (\mathrm{R22})$$

Chlorite will then continue to oxidize the substrate with the same

SCHEME 1: Schematic Representation of Reaction R20

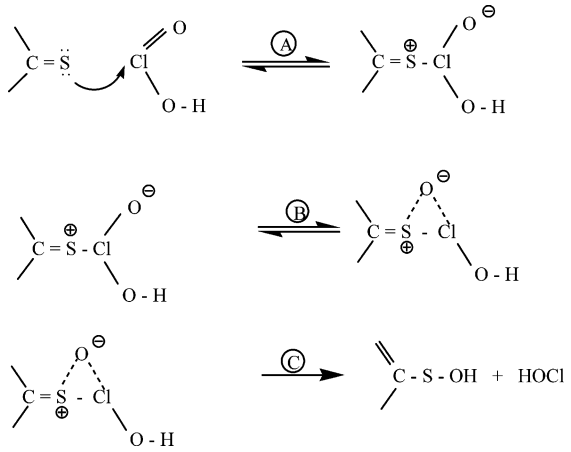

mechanism detailed above, culminating in an autocatalytic consumption of ACTU. This route, however, will require the concomitant formation of thiyl radicals[59] which will undergo a dimerization and further oxidation of the dimeric species through S-oxygenation of the oxo-acids. Without metal ions to mediate thiyl radical formation, the radical pathway should not be dominant. The only viable route is the direct reaction of chlorine dioxide with ACTU. The sulfur center of ACTU is electron rich, and the chlorine center of chlorine dioxide is electron deficient, has an unpaired electron, and possesses a strong formal positive charge. The formation of an adduct between chlorine dioxide and a nucleophile has been widely reported in the literature.[60−62] The formation of an adduct between these two molecules should be energetically favored

$$\mathrm{ClO_2(aq)} + \mathrm{CH_3CONH(NH_2)C{=}S} \rightleftharpoons [\mathrm{CH_3CONH(NH_2)C{=}S{:}ClO_2}];\ k_5;\ k_{-5} \quad (\mathrm{R23})$$

The break-up of the adduct in reaction R23 is solvent assisted and does not involve another $\mathrm{ClO_2}$ molecule. It can also be general-base catalyzed. This was proved by running some experiments in aprotic acetonitrile as solvent. The reaction solutions run in acetonitrile contained approximately 3% v/v water which was derived from the water used to dissolve $\mathrm{ClO_2}$. Figure 9 shows that reactions run in 100% water were much faster than those run in 97% acetonitrile. The proposed reaction scheme for the reaction between chlorine dioxide and ACTU is shown as Scheme 2 (in which ACTU is abbreviated as >C=S). It is important that the breakup of the adduct should occur before the addition of the second $\mathrm{ClO_2}$ molecule since the kinetics data indicate that the reaction is first order in both ACTU and $\mathrm{ClO_2}$. The overall stoichiometry of this rate-determining step is given by reaction R24

$$\mathrm{CH_3CONH(NH_2)C{=}S} + 2\mathrm{ClO_2} + \mathrm{H_2O} \rightarrow \mathrm{CH_3CON{=}(NH_2)CSOH} + 2\mathrm{ClO_2}^- + 2\mathrm{H}^+;\ \text{fast, irreversible} \quad (\mathrm{R24})$$

If one assumes that reaction R23 will not occur (or is exceedingly slow) with a protonated thiocarbamide molecule, then the acid retardation can easily be justified with a rate law of

$$\frac{-\mathrm{d[ClO_2]}}{\mathrm{d}t} = \frac{k_5[\mathrm{ClO_2}][\mathrm{ACTU}]}{1 + K_\mathrm{b}[\mathrm{H}^+]} \quad (4)$$

After R24, the rest of the mechanism becomes essentially that

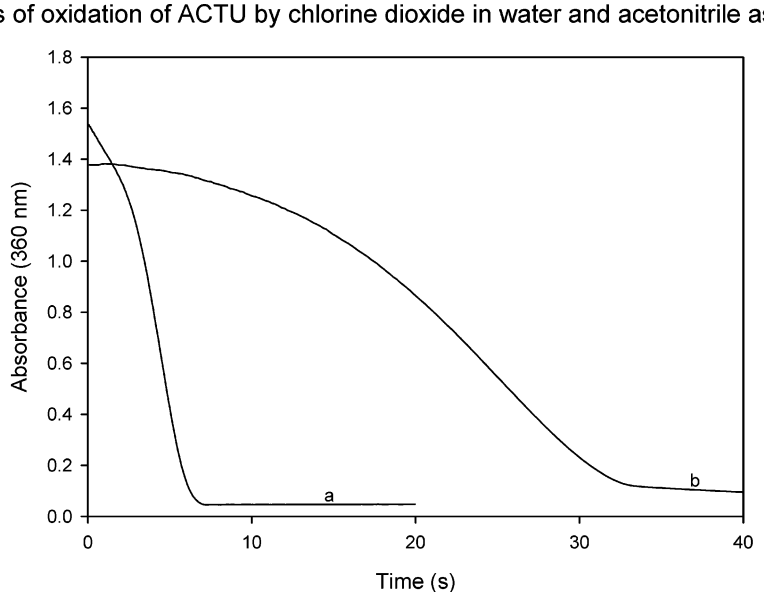

Figure 9. Comparison of rates of oxidation of ACTU by chlorine dioxide in water and acetonitrile/water. Both traces a and b have $[ACTU]_0 = 5.25 \times 10^{-2}$ M, while a has $[ClO_2]_0 = 1.19 \times 10^{-3}$ M and 100% water as reaction medium and b has $[ClO_2]_0 = 1.10 \times 10^{-4}$ M and 97% v/v acetonitrile/water. The reaction run in the protic solvent is much faster than the one run in predominantly the aprotic solvent.

SCHEME 2: Formation and Break-Up of the ACTU−ClO_2 Adduct to Form the Sulfenic Acid and Chlorous Acid

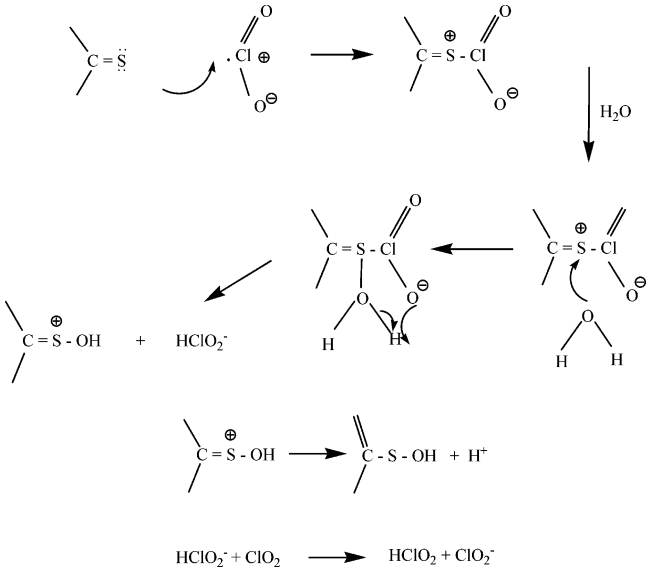

SCHEME 3: Mechanistic Basis of the Direct Oxidation of the Zwitterionic Sulfinic Acid Species to Acetylurea without Passing through the Sulfonic Acid

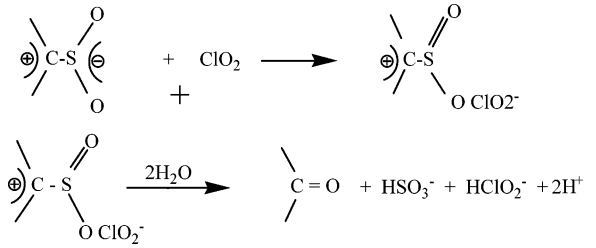

of the chlorite−ACTU reaction. The important feature of Scheme 2 (and Scheme 3 profiled later) is the proposed Cl(II) intermediate, $HClO_2^-$, which should rapidly combine with a ClO_2 molecule in a diffusion-controlled rate to produce two Cl(III) molecules.

Mechanistic Basis of ACTU Consumption. This is characterized by sigmoidal autocatalytic decay kinetics both with ClO_2^- and ClO_2 as oxidants. Data in parts a and b of Figure 5 indicate that the consumption of ACTU occurs in two distinct steps: one initial autocatalytic and rapid step, followed by a slower, nonautocatalytic step. Our kinetics data have shown facile oxidations of the dimeric species, >C−S−S−C<, and the sulfinic acid species by both ClO_2^- and ClO_2. However, sulfonic acids of thiourea and dimethylthiourea are essentially inert to further oxidation. This suggests that reactions R8, R9, and R10 are relatively rapid while reactions of type R11 are slow.

We assume that the primary route of oxidation of the sulfonic acid is via an initial hydrolysis

$$CH_3CON{=}(NH_2)CSO_3H + H_2O \rightarrow CH_3CONH(NH_2)C{=}O + HSO_3^- + H^+ \quad \text{(R25)}$$

All experimental data in this work and in previous research work have indicated that R25 is the dominant pathway in the oxidation of α- and β-aminosulfonic acids.[63] Recent results from our laboratory have also indicated that the sulfonic acid is much more stable in acidic media and would decompose more rapidly in mildly acidic and basic media.[38,64,65] The reactivity of sulfinic and sulfonic acids in the presence of base or other nucleophiles is well known in organic synthesis as the preferred method for guanidylation which involves the elimination of the sulfur oxoacid group.[66−68] A nucleophilic attack on the carbon atom bonded to the sulfonic acid group (a solvent water molecule, for example) would encourage the heterolytic cleavage of the C−S bond to yield a highly reducing sulfur leaving group as in reaction R25. The end of the autocatalytic phase in the consumption of ACTU can be explained by the inertness of the sulfonic acid to further oxidation.

Sequence R5, R8−R11. If the oxidation of the sulfonic acid is slow, then it should be the rate-determining step in the overall oxidation of ACTU. Our kinetics data, however, suggest that oxidation of the sulfinic acid (see Figure 8b) can also proceed directly to acetylurea without having to go through the sulfonic acid. The relative rates of oxidation through the sulfonic acid

TABLE 1: Chlorite−Chlorine Dioxide−ACTU Reaction

no.	reaction[a]	k_f; k_r[b,c]
M1	$ClO_2^- + H^+ \rightarrow HClO_2$	1×10^9; 1.91×10^7
M2	$OCl^- + H^+ \rightarrow HOCl$	1×10^9, 5.2×10^2
M3	$R_1R_2C{=}S + H^+ \rightarrow [R_1R_2C{=}S\text{-}H]^+$	1.1×10^7; 1.0×10^9
M4	$ClO_2^- + R_1R_2C{=}S \rightarrow R_1R_2CSOH + OCl^-$	2.7
M5	$HClO_2 + R_1R_2C{=}S \rightarrow R_1R_2CSOH + HOCl$	12.5
M6	$HClO_2 + [R_1R_2C{=}S{-}H]^+ \rightarrow R_1R_2CSOH + HOCl + H^+$	1.15
M7	$ClO_2^- + HOCl + H^+ \rightleftharpoons Cl_2O_2 + H_2O$	1.01×10^6; 1.0×10^{-1}
M8	$Cl_2O_2 + ClO_2^- \rightleftharpoons 2ClO_2(aq) + Cl^-$	1.5×10^3; 5.5×10^6
M9	$Cl_2O_2 + R_1R_2C{=}S + H_2O \rightarrow R_1R_2CSOH + 2HOCl$	1.25×10^2
M10	$Cl_2O_2 + R_1R_2CSOH + H_2O \rightarrow R_1R_2CSO_2H + 2HOCl$	5.0×10^4
M11	$Cl_2O_2 + R_1R_2CSO_2H + H_2O \rightarrow R_1R_2CSO_3H + 2HOCl$	1.0×10^4
M12	$Cl_2O_2 + R_1R_2CSO_3H + H_2O \rightarrow R_1R_2C{=}O + SO_4^{2-} + 2HOCl + 2H^+$	1.0×10^{-3}
M13	$HOCl + R_1R_2C{=}S \rightarrow R_1R_2CSOH + H^+ + Cl^-$	1.0×10^6
M14	$HOCl + R_1R_2CSOH \rightarrow R_1R_2CSO_2H + H^+ + Cl^-$	8.0×10^5
M15	$HOCl + R_1R_2CSO_2H \rightarrow R_1R_2CSO_3H + H^+ + Cl^-$	5.0×10^3
M16	$HOCl + R_1R_2CSO_3H + H_2O \rightarrow R_1R_2C{=}O + SO_4^{2-} + 3H^+ + Cl^-$	1.0×10^{-2}
M17	$ClO_2^- + R_1R_2CSOH \rightarrow R_1R_2CSO_2H + OCl^-$	1×10^3
M18	$ClO_2^- + R_1R_2CSO_2H \rightarrow R_1R_2CSO_3H + OCl^-$	5.0×10^{-1}
M19	$ClO_2^- + R_1R_2CSO_3H + H_2O \rightarrow R_1R_2C{=}O + SO_4^{2-} + OCl^- + 2H^+$	1×10^{-1}
M20	$HClO_2 + R_1R_2CSOH \rightarrow R_1R_2CSO_2H + HOCl$	5×10^3
M21	$HClO_2 + R_1R_2CSO_2H \rightarrow R_1R_2CSO_3H + HOCl$	2×10^2
M22	$HClO_2 + R_1R_2CSO_3H \rightarrow R_1R_2C{=}O + SO_4^{2-} + HOCl$	1.0×10^{-3}
M23	$R_1R_2CSO_3H + (H_2O) \rightarrow R_1R_2C{=}O + HSO_3^- + H^+$	5.1
M24	$HSO_3^- + ClO_2^- \rightarrow SO_4^{2-} + HOCl$	5.0×10^4
M25	$HSO_3^- + HClO_2 \rightarrow SO_4^{2-} + HOCl + H^+$	1.0×10^5
M26	$HSO_3^- + HOCl \rightarrow SO_4^{2-} + 2H^+ + Cl^-$	5.0×10^6
M27	$HSO_3^- + ClO_2 + (H_2O) \rightarrow SO_4^{2-} + HClO_2^- + 2H^+$	5.0×10^8
M28	$ClO_2(aq) + R_1R_2C{=}S + (H_2O) \rightarrow R_1R_2CSOH + HClO_2^- + 2H^+$	2.0×10^5
M29	$ClO_2(aq) + R_1R_2CSO_2H \rightarrow R_1R_2C{=}O + HSO_3^- + HClO_2^- + 2H^+$	3.25×10^2
M30	$HClO_2^- + ClO_2(aq) \rightarrow HClO_2 + ClO_2^-$	1.0×10^9
M31	$2\ R_1R_2CSOH \rightleftharpoons R_1R_2CSO_2H + R_1R_2C{=}S$	2.0×10^2

[a] Legend: $R_1 = CH_3CONH$; $R_2 = NH_2$; $R_1 = CH_3CON{=}$. [b] Forward and reverse rate constants are separated by a semicolon, where appropriate. [c] Units for kinetics constants are deduced from the molecularity of the reaction except where water is involved as a reactant. In this case its activity is assumed to be unity.

compared to direct oxidation to acetylurea is determined by the pH, with low pH conditions favoring oxidation through the sulfonic acid. This assertion can be proved by previous work from our laboratories in which acid retards the oxidation of cysteinesulfinic acid by chlorine dioxide.[39] Scheme 3 details a mechanism in which chlorine dioxide oxidizes the sulfinic acid directly to urea, bypassing the sulfonic acid. β-Aminosulfonic acids exist as zwitterions,[38] and thus Scheme 3 involves an initial reaction between the sulfinic acid center and chlorine dioxide. The overall stoichiometry of this two-electron oxidation is

$$CH_3CON{=}(NH_2)CSO_2H + 2ClO_2 + H_2O \rightarrow CH_3CONH(NH_2)C{=}O + HSO_3^- + 2HClO_2 + H^+ \quad \text{(R26)}$$

Further oxidation of HSO_3^- is rapid

$$ClO_2^- + HSO_3^- \rightarrow HOCl + SO_4^{2-} \quad \text{(R27)}$$

$$HOCl + HSO_3^- \rightarrow SO_4^{2-} + 2H^+ + Cl^- \quad \text{(R28)}$$

Chlorine Dioxide Formation. Reaction R7 is responsible for formation of ClO_2. This reaction is initiated by reaction R5 and any other reactions that reduce ClO_2^- to HOCl. There is an immediate competition set up between reactions R7 and R8−R10 for HOCl. If reactions that consume ClO_2 are fast (e.g., R24), then formation of ClO_2 will only commence after total consumption of ACTU and its metabolites. In the ClO_2^-−ACTU reaction, reactions that form ClO_2 and those that consume ClO_2 are comparable in rate, and assertion of each set of reactions depends on availability of reagents that fuel these sets of reactions. The autocatalytic nature of the formation of HOCl means that (i) a faster oxidation rate by ClO_2^- (e.g., reaction R5) would lead to a faster rate of formation of ClO_2 and (ii) a slower rate of oxidation by ClO_2 means a higher rate of formation of ClO_2. In Figure 2, the initial phase of the reaction involves oxidation of ACTU by ClO_2^- to yield HOCl, which forms ClO_2 from ClO_2^- and also oxidizes ACTU and its metabolites. The resultant is a slow accumulation of ClO_2. The sudden increase in the rate of formation of ClO_2 indicates oxidation of ACTU past the sulfinic acid stage (up to reaction R10, for example). Since reaction R11 is slow, formation of ClO_2 will proceed autocatalytically without its concomitant consumption. This analysis is corroborated by data shown in Figure 5c in which ClO_2 formation commences at the end of the autocatalytic consumption of ACTU (i.e., at the point of formation of the sulfonic acid).

Computer Simulations. A single reaction network mechanism can be derived for both the ClO_2^-−ACTU and ClO_2−ACTU reactions because both reactions are relevant in the overall mechanism at any time. By altering initial conditions, the adopted mechanism was able to simulate both reaction systems. A general mechanism derived for this chemical system is shown in Table 1. In highly acidic conditions, some reactions listed in this table were insignificant and could be removed from the scheme. This includes reactions M4 and M17−M19. The adopted mechanism in Table 1 consists of three rapid protolytic equilibria (M1−M3), three initiation reactions (M4−M6), and a series of reactions that involve the oxidation of a sulfur center coupled to the reduction of a chlorine center (M4−M6, M9−M22, M24−M30). While Table 1 nearly caters for the full combination of 4 oxidants (ClO_2, ClO_2^-, $HClO_2$, and HOCl) with all five possible reductants in the reaction medium (ACTU and its oxo-acids as well as HSO_3^-), we take advantage of the autocatalysis mechanism to utilize oxidations by HOCl only.

Such an implementation introduced a small error in the whole simulations because HOCl oxidations become dominant as the reaction proceeds, although during the initial stages oxidations by $HClO_2$ and ClO_2^- will be more dominant. The mechanism shown in Table 1 includes the hydrolysis of the sulfonic acid to give bisulfite (reaction M23). Previous work by us and others have confirmed that reaction M23 is the dominant pathway by which α- and β-aminosulfonic acids are oxidized since reactions M16, M19, and M22 have experimentally been proved to be slow.[38,63,69] Reaction M23 is very slow in highly acidic conditions and is much more rapid in basic environments. Production of HSO_3^- introduces rapid reactions M24, M25, and M27, which rapidly convert ClO_2^- and ClO_2 to HOCl. Removal of this set of rapid reactions from the reaction scheme did not allow the mechanism to display the rapid autocatalytic decay observed in parts a and b of Figure 5 and Figures 6a and 7. Reaction M31 was added for stoichiometric consistency in conditions of excess reductant. By making it slow, it became relevant only at the end of the reaction and was not effective in the first 5 s of the reaction.

Selection of Rate Constants. Reactions M1−M3 were considered to be rapid, protolytic, and diffusion controlled. The specific values of the rate constants themselves were not important for as long as they were fast enough so as not to be rate determining and that acid dissociation constant values were adhered to. By setting the forward rate constants for M1 and M2, the reverse rate constants were then fixed by $pK_a(HClO_2) = 1.72$ and $pK_a(HOCl) = 7.49$,[70] respectively. The value of K_b of the thiocarbamide was initially guessed using a previous value determined in our laboratories for guanythiourea[71] and then refined to fit the data at high acid concentrations. For most of the simulations, which were performed at acid concentrations of less that 0.05 M, the protonation of ACTU (reaction M3) was not significant. The most important kinetics parameters were those for reactions M4 and M5 as they represent the initiation reactions. The strongly autocatalytic nature of the reaction made it difficult to experimentally obtain accurate estimates of k_{M4} and k_{M5}. The values adopted for simulating the induction period shown in Figure 3a were 2.70 and 12.5 M^{-1} s^{-1}, respectively, for k_{M4} and k_{M5}. The procedure used to evaluate these important rate constants involved initially fitting experimental data at high acid concentrations such as in Figure 3b in which ClO_2^- concentrations were negligible, thereby rendering reaction M3 ineffective. In this mode, we only had to fit k_{M5}. This upper limit value of k_{M5} was then used to fit low acid concentration data such as in Figure 3a, and in this way k_{M4} was then established. Reaction M6 was not effective in this mechanism and could be omitted. It has an insignificant contribution to the initiation of the reaction. Kinetics parameters for M7 and M8 were obtained from the literature.[32] Reactions M9 to M12 represented the autocatalytic HOCl production. The simulations were supposed to keep the autocatalytic species concentrations low. This precondition appeared essential for the establishment of HOCl autocatalysis in which the rate of oxidation of ACTU and its metabolites becomes dependent on the rate of autocatalytic production of HOCl, and hence the sigmoidal decay kinetics. Oxidations of the sulfonic acid, reactions M12, M16, M19, and M22, were deliberately retained at very low and insignificant values such that the main oxidation process of the sulfonic acid was mainly through its hydrolysis (reaction M23). Rate of M13 was estimated by the use of a recent study that evaluated a bimolecular oxidation rate constant[72] of cysteine by HOCl as 2.0×10^5 M^{-1} s^{-1}. We adopted a rate constant of 1.0×10^6 M^{-1} s^{-1}. Because of the consecutive nature of these

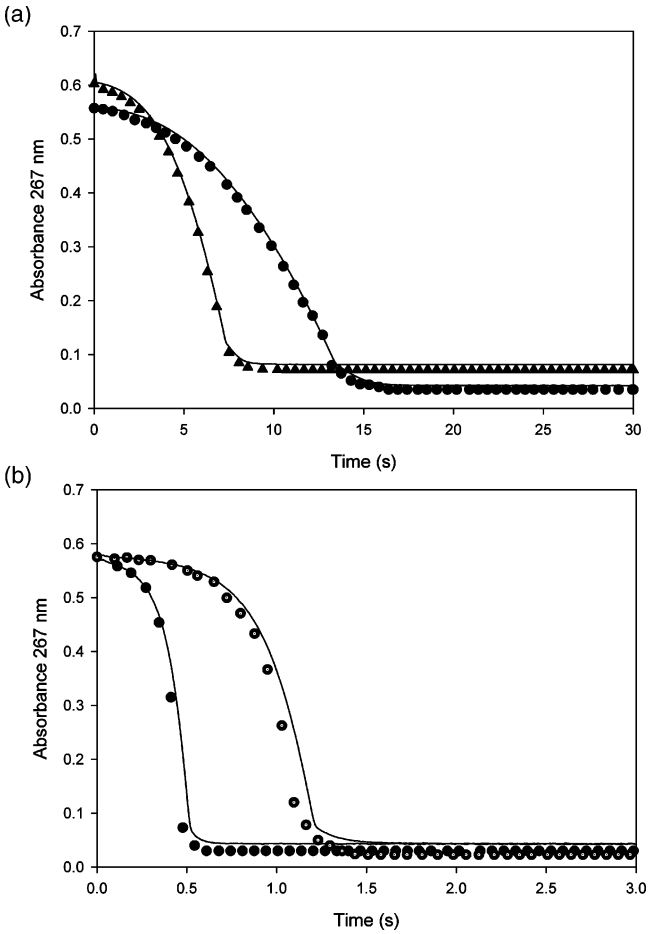

Figure 10. (a) Comparison of experimental and calculated curves from Figure 5a. There is a very adequate fit to the experimental data. $[ACTU]_0 = 4.0 \times 10^{-5}$ M, $[H^+]_0 = 2.5 \times 10^{-2}$ M. $[ClO_2^-]_0$ = (a) 7.5×10^{-4} M, (b) 1.5×10^{-3} M. (b) Comparison of experimental and calculated curves for data shown in Figure 7 for the oxidation of ACTU by chlorine dioxide. $[ACTU]_0 = 4.0 \times 10^{-5}$ M, $[ClO_2]_0 = 4.95 \times 10^{-4}$ M, $[H^+]_0$ = (a) 0.01 M, (b) 0.03 M.

sets of reactions, the most important rate constants were the initial and slowest ones in the chains: M13−M16, M4, M17−M19, M5, and M20−M22. Reactions M27−M30 involve oxidations by ClO_2. Parameters for reaction M28 were the most important in determining the overall reaction dynamics of chlorine dioxide consumption. The kinetics parameters for reaction M28 could not be estimated from the pseudo-first order plots (Supporting Information Figure 3Sc). These data gave a very low bimolecular rate constant of only 3.0 M^{-1} s^{-1} because they were run in excess acid in which the ACTU was protonated. The actual value adopted that allowed for the simulation of data shown in Figures 6a and 7 was 5.0×10^4 M^{-1} s^{-1}. Reaction M27 was initially guessed from a comparable study of the oxidation of thiosulfate by chlorine dioxide.[62]

The mechanism's biggest handicap was the inability to estimate k_{M23}. This is a strongly pH- and solvent-dependent value. The value adopted for this hydrolysis was only relevant within the small range of acid concentrations used to simulate parts a and b of Figure 10. Outside this range, a different hydrolysis rate constant would have had to be adopted. Production of HSO_3^- contributed to the autocatalysis by immediately producing ClO_2^- from ClO_2.

Reaction scheme in Table 1 was simulated using the Kintecus Integrator developed by James Ianni.[73] Most of the dynamics displayed by the reaction could be satisfactorily modeled by this scheme. Both chlorite and chlorine dioxide oxidations could

be simulated by the same scheme by merely altering the initial conditions to suit the specific oxidation to be simulated. Although the mechanism could simulate the oligo-oscillatory behavior shown in Figure 4a, it could not reproduce the very sharp concentrations changes observed. We surmise that the most important reactions needed for the generation of these oligo-oscillations may be M23, M28, and M29. The decomposition of the sulfonic acid has only been recently discovered, and the kinetics of this process are still unknown.[64,65] Parts a and b of Figure 10show acceptable fits to the experimental data. Figure 10a involves formation of chlorine dioxide at the end of ACTU consumption. This chlorine dioxide contributed to the absorbance observed experimentally at the end of the reaction. This contribution was added to the absorbance deduced from the calculations for the observed fit.

Conclusion

This study has shown that the small substitution of an acetyl group on the parent thiourea compound can produce a vastly different oxidation mechanism. The reaction of chlorite and thiourea was much slower and did not have as strong autocatalysis as the corresponding oxidation of ACTU profiled in this manuscript. The addition of the acetyl group is enough to alter the oxidation mechanism. The oligo-oscillatory dynamics observed with ACTU were not observed with thiourea. This would be reflected in varied metabolic activation mechanisms possibly leading to different physiological effects from very similar thiocarbamides.

Acknowledgment. We would like to thank the National Institute for Occupational Safety and Health (Health Effects Laboratory) for hosting and financially supporting O.O. during the major part of this study. This work was also supported by Grant Nos. CHE-0137435, CHE 0341769, and OISE 0422689 from the National Science Foundation.

Supporting Information Available: Under Supporting Information the reader will find a series of kinetics data not listed among the figures presented in this manuscript. This file also contains UV/vis spectra of the reagents and products. All figures in the Supporting Information are mentioned in the body of the manuscript. This material is available free of charge via the Internet at http://pubs.acs.org.

References and Notes

(1) Part 7 (of 10) in the series of publications to honor the memory of Dr. Cordelia R. Chinake (1965−1998). Part 6: Madhiri, N.; Olojo, R.; Simoyi, R. H. Oxyhalogen−Sulfur Chemistry: Kinetics and Mechanism of Oxidation of Formamidine Disulfide by Acidic Bromate. *Phys. Chem. Chem. Phys.* **2003**, *5* (19), 4149−4156.

(2) Ziegler-Skylakakis, K.; Nill, S.; Pan, J. F.; Andrae, U. *Environ. Mol. Mutagen.* **1998**, *31*, 362−373.

(3) Jirousek, L.; Soodak, M. *J. Pharmacol. Exp. Ther.* **1974**, *191*, 341−348.

(4) Simoyi, R. H. *J. Phys. Chem.* **1986**, *90*, 2802−2804.

(5) Doona, C. J.; Blittersdorf, R.; Schneider, F. W. *J. Phys. Chem.* **1993**, *97*, 7258−7263.

(6) Chinake, C. R.; Simoyi, R. H. *J. Chem. Soc., Faraday Trans.* **1997**, *93*, 1345−1350.

(7) Orban, M.; Epstein, I. R. *J. Am. Chem. Soc.* **1992**, *114*, 1252−1256.

(8) Rabai, Gy.; Orban, M.; Epstein, I. R. *Acc. Chem. Res.* **1990**, *23*, 258−263.

(9) Davies, M. J.; Hawkins, C. L. *Free Radical Res.* **2001**, *33*, 719−729.

(10) Licht, S.; Gerfen, G. J.; Stubbe, J. *Science* **1996**, *271*, 477−481.

(11) Kalyanaraman, B. *Biochem. Soc. Symp.* **1995**, *61*, 55−63.

(12) Shi, X. L.; Sun, X. Y.; Dalal, N. S. *FEBS Lett.* **1990**, *271*, 185−188.

(13) Simoyi, R. H.; Epstein, I. R. *J. Phys. Chem.* **1987**, *91*, 5124−5128.

(14) Jones, J. B.; Chinake, C. R.; Simoyi, R. H. *J. Phys. Chem.* **1995**, *99*, 1523−1529.

(15) Martincigh, B. S.; Hauser, M. J. B.; Simoyi, R. H. *Phys. Rev. E* **1995**, *52*, 6146−6153.

(16) Chinake, C. R.; Mambo, E.; Simoyi, R. H. *J. Phys. Chem.* **1994**, *98*, 2908−2916.

(17) Mambo, E.; Simoyi, R. H. *J. Phys. Chem.* **1993**, *97*, 13662−13667.

(18) Safaev, R. D.; Voronkov, M. G.; Fuks, S. I.; Lycheva, T. A.; Khitrovo, I. A.; Belitskii, G. A.; Pakhomov, V. I.; Vlasova, N. N.; Pestunovich, A. E. *Dokl. Akad. Nauk* **1992**, *322*, 994−996.

(19) Stevens, G. J.; Hitchcock, K.; Wang, Y. K.; Coppola, G. M.; Versace, R. W.; Chin, J. A.; Shapiro, M.; Suwanrumpha, S.; Mangold, B. L. *Chem. Res. Toxicol.* **1997**, *10*, 733−741.

(20) Guo, W. X.; Poulsen, L. L.; Ziegler, D. M. *Biochem. Pharmacol.* **1992**, *44*, 2029−2037.

(21) Salem, M. A.; Chinake, C. R.; Simoyi, R. H. *J. Phys. Chem.* **1996**, *100*, 9377−9384.

(22) Kearns, S.; Dawson, R., Jr. *Adv. Exp. Med. Biol.* **2000**, *483*, 563−570.

(23) Mrakavova, M.; Melichercik, M.; Olexova, A.; Treindl, L. *Collect. Czech. Chem. Commun.* **2003**, *68*, 23−34.

(24) Martincigh, B. S.; Simoyi, R. H. *J. Phys. Chem. A* **2002**, *106*, 482−489.

(25) Kern, D.; Kim, C.-H. *J. Am. Chem. Soc.* **1965**, *87*, 5309−5313.

(26) Lengyel, I.; Li, J.; Kustin, K.; Epstein, I. R. *J. Am. Chem. Soc.* **1996**, *118*, 3708−3719.

(27) Horvath, A. K.; Nagypal, I.; Peintler, G.; Epstein, I. R.; Kustin, K. *J. Phys. Chem. A* **2003**, *107*, 6966−6973.

(28) Blake, D. R.; Hall, N. D.; Bacon, P. A.; Dieppe, P. A.; Halliwell, B.; Gutteridge, J. M. *Ann. Rheum. Dis.* **1983**, *42*, 89−93.

(29) Chinake, C. R.; Simoyi, R. H. *J. Phys. Chem.* **1994**, *98*, 4012−4019.

(30) Brauer, G. *Handbook of Preparative Organic Chemistry*; Academic Press: New York, 1963; p 301.

(31) Chinake, C. R.; Olojo, O.; Simoyi, R. H. *J. Phys. Chem. A* **1998**, *102*, 606−611.

(32) Peintler, G.; Nagypal, I.; Epstein, I. R. *J. Phys. Chem.* **1990**, *94*, 2954−2960.

(33) Chinake, C. R.; Simoyi, R. H. *J. Phys. Chem. B* **1997**, *101*, 1207−1214.

(34) Epstein, I. R.; Kustin, K.; Simoyi, R. H. *J. Phys. Chem.* **1992**, *96*, 5852−5856.

(35) Chinake, C. R.; Simoyi, R. H. *J. Phys. Chem.* **1993**, *97*, 11569−11570.

(36) Cotton, F. A.; Wilkinson, G. *Advanced Inorganic Chemistry*, 5th ed.; Wiley-Interscience: New York, 1988; p 567.

(37) Rabai, G.; Beck, M. T. *J. Chem. Soc., Dalton Trans.* **1985**, 1669−1672.

(38) Makarov, S. V.; Mundoma, C.; Penn, J. H.; Petersen, J. L.; Svarovsky, S. A.; Simoyi, R. H. *Inorg. Chim. Acta* **1999**, *286*, 149−154.

(39) Darkwa, J.; Olojo, R.; Chikwana, E.; Simoyi, R. H. *J. Phys. Chem. A* **2004**, *108*, 5576−5587.

(40) Rabai, G.; Orban, M. *J. Phys. Chem.* **1993**, *97*, 5935−5939.

(41) Stanbury, D. M.; Finglar, J. N. *Coord. Chem. Rev.* **1999**, *187*, 223−232.

(42) Karoui, H.; Hogg, N.; Frejaville, C.; Tordo, P.; Kalyanaraman, B. *J. Biol. Chem.* **1996**, *271*, 6000−6009.

(43) Scorza, G.; Minetti, M. *Biochem. J.* **1998**, *329*, 405−413.

(44) Darkwa, J.; Olojo, R.; Olagunju, O.; Otoikhian, A.; Simoyi, R. *J. Phys. Chem. A* **2003**, *107*, 9834−9845.

(45) Jonnalagadda, S. B.; Chinake, C. R.; Olojo, R.; Simoyi, R. H. *Int. J. Chem. Kinet.* **2002**, *34*, 237−247.

(46) Poulsen, L. L.; Hyslop, R. M.; Ziegler, D. M. *Arch. Biochem. Biophys.* **1979**, *198*, 78−88.

(47) Kustin, K.; Eigen, M. *J. Am. Chem. Soc.* **1962**, *84*, 1355−1359.

(48) Simoyi, R. H.; Epstein, I. R.; Kustin, I. *J. Phys. Chem.* **1994**, *98*, 551−557.

(49) Jia, Z.; Margerum, D. W.; Francisco, J. S. *Inorg. Chem.* **2000**, *39*, 2614−2620.

(50) Magee P. S. *Sulfur in Organic and Inorganic Chemistry*; M. Dekker: New York, 1971; Chapter 9.

(51) Okazaki, R.; Goto, K. *Heteroatom Chemistry* **2002**, *13*, 414−418.

(52) Capozzi G.; Modena, G. *The Chemistry of the Thiol Group*, 5th ed.; Wiley-Interscience: New York, 1974; pp 791−796.

(53) Madhiri, N.; Olojo, R.; Simoyi, R. H. *Phys. Chem. Chem. Phys.* **2003**, *5*, 4149−4156.

(54) Taube, H.; Dodgen, H. *J. Am. Chem. Soc.* **1949**, *71*, 3330−3336.

(55) Rabai, G.; Orban, M. *J. Phys. Chem.* **1993**, *97*, 5935−5939.

(56) Furman, C. S.; Jia, Z. J.; Margerum, D. W. *Abstracts of Papers of the American Chemical Society* **1998**, *216*, U98.

(57) Fabian, I.; Szucs, D.; Gordon, G. *J. Phys. Chem. A* **2000**, *104*, 8045−8049.

(58) Tratnyek, P. G.; Hoigne, J. *Water Res.* **1994**, *28*, 57−66.
(59) Rabai, G.; Wang, R. T.; Kustin, K. *Int. J. Chem. Kinet.* **1993**, *25*, 53−62.
(60) Fabian, I.; Gordon, G. *Inorg. Chem.* **1997**, *36*, 2494−2497.
(61) Horvath, A. K.; Nagypal, I.; Epstein, I. R. *J. Phys. Chem. A* **2003**, *107*, 10063−10068.
(62) Horvath, A. K.; Nagypal, I. *J. Phys. Chem. A* **1998**, *102*, 7267−7272.
(63) Makarov, S. V.; Mundoma, C.; Penn, J. H.; Svarovsky, S. A.; Simoyi, R. H. *J. Phys. Chem. A* **1998**, *102*, 6786−6792.
(64) Chigwada, T. R.; Chikwana, E.; Simoyi, R. H. *J. Phys. Chem. A* **2005**, *109*, 1081−1093.
(65) Chigwada, T. R.; Simoyi, R. H. *J. Phys. Chem. A* **2005**, *109*, 1094−1104.
(66) Kim, K.; Lin, Y.-T.; Mosher, H. S. *Tetrahedron Lett.* **1988**, *26*, 3183−3186.
(67) Maryanoff, C. A.; Stanzione, R. C.; Plampin, J. N.; Mills, J. E. *J. Org. Chem.* **1986**, *51*, 1882−1884.
(68) Yong, Y. F.; Kowalski, J. A.; Lipton, M. A. *J. Org. Chem.* **1997**, *62*, 1540−1542.
(69) Ojo, J. F.; Otoikhian, A.; Olojo, R.; Simoyi, R. H. *J. Phys. Chem. A* **2004**, *108*, 2457−2463.
(70) Hwang, E.; Cash, J. N.; Zabik, M. J. *J. Agric. Food Chem.* **2002**, *50*, 4734−4742.
(71) Chikwana, E.; Simoyi, R. H. *J. Phys. Chem. A* **2004**, *108*, 1024−1032.
(72) Peskin, A. V.; Winterbourn, C. C. *Free Radical Biol. Med.* **2001**, *30*, 572−579.
(73) Ianni, J. C. Kintecus: The Kinetics Program Modules for the Ultimate Lazy Scientist. http://www.theochem.kth.se/html/pemac/links/KINTECUS.en.html, 1996.